IOSR Journal of Applied Physics (IOSR-JAP)
e-ISSN: 2278-4861.Volume 18, Issue 3 Ser. 1 (May – June 2026), PP 50-59
www.iosrjournals.org

Exploring a Solar Flare Using Multi-wavelength Observations and Extrapolation of Surface Magnetic Field

Divya Kumari and Alok Ranjan Tiwary*
University Department of Physics, Jai Prakash University, Chapra, Bihar, India
**Corresponding Author: Alok Ranjan Tiwary*

Abstract
We present a detailed multiwavelength analysis of a confined solar flare that took place on 13 February 2016 in NOAA Active Region 2497. The flare was linked to significant EUV brightenings, the development of hot coronal loops, and considerable restructuring of magnetic field lines; however, no successful coronal mass ejection (CME) was detected, thereby confirming the confined nature of the event. The multiwavelength observations suggest intense high-temperature emissions concentrated around the flare core region, signifying considerable plasma heating resulting from magnetic reconnection. Moreover, observations indicated increased chromospheric and transition-region brightenings, along with localized plasma movements and evolving loop structures throughout the flare's progression. To explore the magnetic topology related to the flare, a pre-flare line-of-sight magnetogram captured at 15:12 UT was employed for potential magnetic field extrapolation. This magnetogram unveiled a complex mixed-polarity magnetic configuration characterized by strong magnetic gradients and polarity inversion regions, which are conducive to magnetic energy storage and reconnection. The extrapolated field lines demonstrated a strong correlation with the observed coronal loops and indicated the existence of a stable overlying magnetic arcade system situated above the flare core region. The findings imply that the robust overlying magnetic field was instrumental in inhibiting the eruption and averting the formation of a CME, despite the significant energy release associated with the flare. This study underscores the significance of coronal magnetic topology and magnetic confinement in comprehending the dynamics and evolution of confined solar flares.

Keywords: *Confined Solar Flare, Magnetic Topology, Observations, Extrapolation, Magnetic reconnection.*

Date of Submission: 25-05-2026 Date of Acceptance: 06-06-2026

I. Introduction

Solar flares represent some of the most powerful expressions of magnetic energy discharge within the solar atmosphere, often linked to abrupt brightenings across the electromagnetic spectrum, heating of plasma, acceleration of particles, and swift reconfiguration of coronal magnetic fields [1–3]. These phenomena arise in magnetically intricate active regions where magnetic free energy is progressively built up through flux emergence, shearing motions, and magnetic interactions occurring near polarity inversion lines [4,5]. Based on their development and magnetic surroundings, solar flares can be categorized as either eruptive or confined events. Eruptive flares are typically associated with coronal mass ejections (CMEs), while confined flares release significant energy without resulting in a successful large-scale eruption into the heliosphere [6–8].

Confined flares are particularly noteworthy as they offer valuable insights into the magnetic conditions that inhibit eruptions, even in the presence of considerable energy release in the corona [9]. In these instances, robust overlying magnetic fields can obstruct the upward expansion of magnetic flux ropes or erupting plasma structures, thus limiting the energy release to the lower corona [10]. Numerous observational and theoretical investigations have indicated that the decay rate and configuration of the overlying magnetic field are critical factors in determining whether a flare becomes eruptive or remains confined [11–13]. Consequently, comprehending the magnetic structure and evolution of confined flares is vital for exploring flare triggering mechanisms and the storage of magnetic energy in solar active regions.

Magnetic reconnection is regarded as the fundamental physical process that facilitates the release of energy during flares in both eruptive and confined events [14,15]. In the course of reconnection, magnetic field lines that are oriented in opposite directions reconnect, swiftly transforming magnetic energy into thermal energy, plasma flows, and energetic particles [16]. The observable indicators of reconnection encompass compact flare brightenings, hot loop arcades, cusp-shaped structures, and dynamic coronal loops that are detected in extreme

ultraviolet (EUV) and X-ray wavelengths [17–19]. Even in confined events, reconnection can lead to substantial plasma heating and considerable restructuring of coronal loops without resulting in a coronal mass ejection (CME) [20].

The Solar Dynamics Observatory has significantly enhanced the comprehension of solar flare dynamics through high-resolution, multiwavelength observations of the solar atmosphere. The Atmospheric Imaging Assembly (AIA) offers full-disk observations across various EUV and UV wavelengths with high temporal and spatial resolution, facilitating a thorough examination of flare evolution from the chromosphere to the corona [21]. Notably, the AIA 131 Å and 94 Å channels are responsive to hot flare plasma and reconnection areas, while the 304 Å channel highlights chromospheric and transition-region responses, including flare ribbons and plasma movements [22]. Concurrently, the Helioseismic and Magnetic Imager (HMI) assesses the photospheric magnetic field, which is crucial for understanding magnetic topology and the magnetic evolution associated with flares [23].

Magnetic field extrapolation methods are extensively employed to recreate the three-dimensional coronal magnetic structure from observed photospheric magnetograms [24]. The potential field extrapolation method presumes a current-free coronal magnetic field and offers significant insights into large-scale magnetic connectivity and loop geometry [25]. While confined flares often involve non-potential magnetic configurations, potential field models continue to be valuable for analyzing the background magnetic topology and identifying the overlying magnetic arcade systems that may obstruct eruptions [26]. Comparisons between extrapolated magnetic field lines and EUV coronal loops captured by AIA assist in elucidating the magnetic environment that influences flare development [27]. Prior studies have shown that confined flares are often linked to robust overlying magnetic arcades, compact loop systems, and restricted upward expansion of hot plasma structures [28–30]. The stability of the overlying coronal field can inhibit the torus instability and prevent the release of magnetic flux ropes, resulting in a confined event despite considerable energy discharge [31]. Consequently, detailed multiwavelength observations, in conjunction with magnetic field extrapolation, are crucial for comprehending the physical mechanisms that govern confined solar flares.

On 13 February 2016, a confined flare took place in NOAA Active Region 2497, displaying intense EUV brightenings, hot coronal loops, and notable magnetic restructuring without leading to a successful large-scale eruption. The event was monitored across multiple AIA channels, facilitating the examination of flare evolution across various atmospheric layers and plasma temperatures. In this study, we investigate the temporal and spatial evolution of the flare utilizing AIA 131 Å, 94 Å, and 304 Å observations alongside HMI magnetograms. Potential magnetic field extrapolation is conducted using the pre-flare HMI magnetogram to reconstruct the coronal magnetic topology and explore the magnetic configuration.

In the following, Section 2 is dedicated for the details of the observations used to explore the flaring event. Section 3 provides the results and discussion using the multi-wavelength analysis and the extrapolation of the event. Section 4 explains a summary of the key findings.

II. Data and Observation

In this work, we explore M1.8 class flare in AR 12497 that occurred on 13 February 2016. The flare started at 15:16 UT, peaked at 15:24 UT and ended at 15:26 UT. In the absence of any associated CME, the flare is found to be confined in nature. For exploring the onset of the flare using imaging, we take into account the data of multiwavelength observations obtained from the AIA aboard the Solar Dynamics Observatory (SDO). To understand the associated surface's magnetic field, we utilize the data from HMI aboard HMI. In particular, for the magnetic field analysis, we use the SpaceWeather HMI Active Region Patch (SHARP) data set, specifically the hmi.sharp_cea_720s data series.

Figure 1 depicts the spatial positioning and temporal development of the solar flare that took place on 13 February 2016, as recorded the AIA/SDO, along with soft X-ray data from the GOES satellite. The upper section features the full-disk solar image captured in the AIA 94 Å channel at 15:25:02 UT, while the lower section presents the corresponding GOES 1–8 Å soft X-ray flux profile linked to the flare event. In the upper section, the solar disk is illustrated with heliographic grid lines that denote the spatial coordinates on the Sun. Several active regions are identified, including AR 12492, AR 12493, AR 12498, and AR 12497. The red rectangular box emphasizes NOAA Active Region 12497, which is the origin of the flare activity. This active region is depicted as a compact bright emission area near the western hemisphere of the solar disk, signifying intense coronal heating and heightened magnetic activity. The AIA 94 Å channel is responsive to hot plasma with temperatures reaching several million Kelvin, making it valuable for pinpointing flare cores and areas of significant magnetic energy

release. The highlighted active region exhibits concentrated EUV emission, indicating the presence of highly energized coronal loops and ongoing magnetic reconnection.

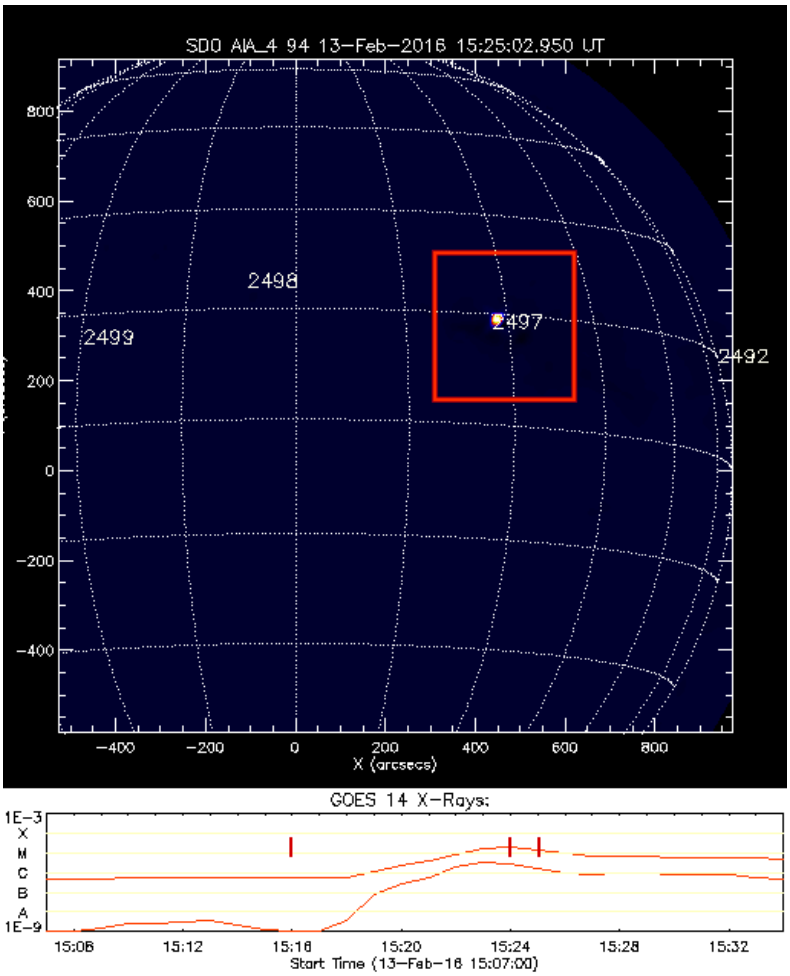

Figure 1: Full-disk solar image observed by the AIA/SDO in the 94 Å channel at 15:25:02 UT on 13 February 2016. The red rectangular box marks AR 12497, identified as the source region of the flare activity. Other active regions present on the solar disk are also labeled. The lower panel shows the corresponding GOES 14 soft X-ray flux profile in the 1–8 Å channel, illustrating the temporal evolution of the associated M-class flare. The vertical red lines indicate important phases of the flare evolution, including the onset and peak emission

The lower panel illustrates the GOES 14 soft X-ray flux profile during the time frame from approximately 15:06 UT to 15:33 UT. The vertical axis indicates the intensity of X-ray flux in watts per square meter on a logarithmic scale, with flare classifications ranging from A, B, C, M, to X levels. The red curve depicts a gradual increase in soft X-ray emission starting around 15:16 UT, followed by a rapid ascent that peaks near 15:24–15:25 UT. The intensity of the flare reaches the M-class level, signifying a moderate yet notable solar flare event. The vertical red markers on the GOES profile highlight significant phases of the flare's evolution, likely corresponding to the onset of the flare, peak emission, and the subsequent decay phase. Following the peak intensity, the X-ray flux gradually diminishes, indicating the cooling of the heated coronal plasma and the transition into the post-flare phase.

III. Result and Discussion

3.1 Multiwavelength Analysis of the Flare

Figure 2 depicts a series of EUV images capturing a solar active region, as observed by the AIA aboard the Solar Dynamics Observatory in the 131 Å wavelength channel on 13 February 2016. The AIA 131 Å channel is primarily designed to observe extremely hot plasma, with temperatures approaching 10 million K, making it particularly effective for investigating flare cores, magnetic reconnection, and eruptive activities within the solar

corona. This sequence demonstrates the temporal progression of the active region throughout the flare and eruption process over an approximate duration of eight minutes. Panel (a), recorded at 15:12:07 UT, illustrates the initial phase of the event prior to the significant eruption. The image displays a complex arrangement of bright coronal loops scattered throughout the active region. A compact bright structure is discernible near the center-right area of the image at coordinates X≈190″ and Y≈130″, indicating substantial heating in the flare core region. Numerous large-scale loop systems extend across the field of view, reflecting a highly sheared and magnetically stressed coronal environment. The diffuse horizontal emission linking various regions implies strong magnetic connectivity within the active region.

In panel (b), captured at 15:16:55 UT, the active region exhibits increased dynamism. The yellow arrow points to a faint feature moving outward in the lower-right section of the image. This structure likely represents the initial expansion of hot coronal plasma or erupting magnetic loops associated with the beginning of the eruption. The flare core remains exceptionally bright, signifying ongoing magnetic energy release and plasma heating through magnetic reconnection. In comparison to panel (a), the surrounding coronal loops appear more disturbed, indicating that the magnetic field configuration is experiencing rapid restructuring.

Panel (c), captured at 15:18:55 UT, illustrates a notable increase in the brightness of the flare core. The dashed yellow box highlights the main eruptive area where intense emissions are concentrated. Within this boxed region, the bright loop-like formation becomes more distinct and compact, signifying significant heating of plasma at flare temperatures. The shape of this bright feature resembles a flare arcade or a twisted magnetic flux system that forms during magnetic reconnection. The enhanced emissions detected in the AIA 131 Å channel clearly indicate the emergence of high-temperature plasma in the reconnection zone. Panel (d), documented at 15:19:55 UT, depicts a more progressed phase of the eruptive event. The green arrow indicates a newly brightened structure located near X≈80″ and Y≈85″, which may be associated with the movement of hot plasma, newly created post-flare loops, or secondary energy release instigated by the changing magnetic configuration. The flare core, enclosed within the dashed box, continues to grow in intensity and expand, suggesting ongoing magnetic reconnection and energy release. The adjacent loop structures also appear increasingly distorted, indicating a large-scale reconfiguration of the coronal magnetic field.

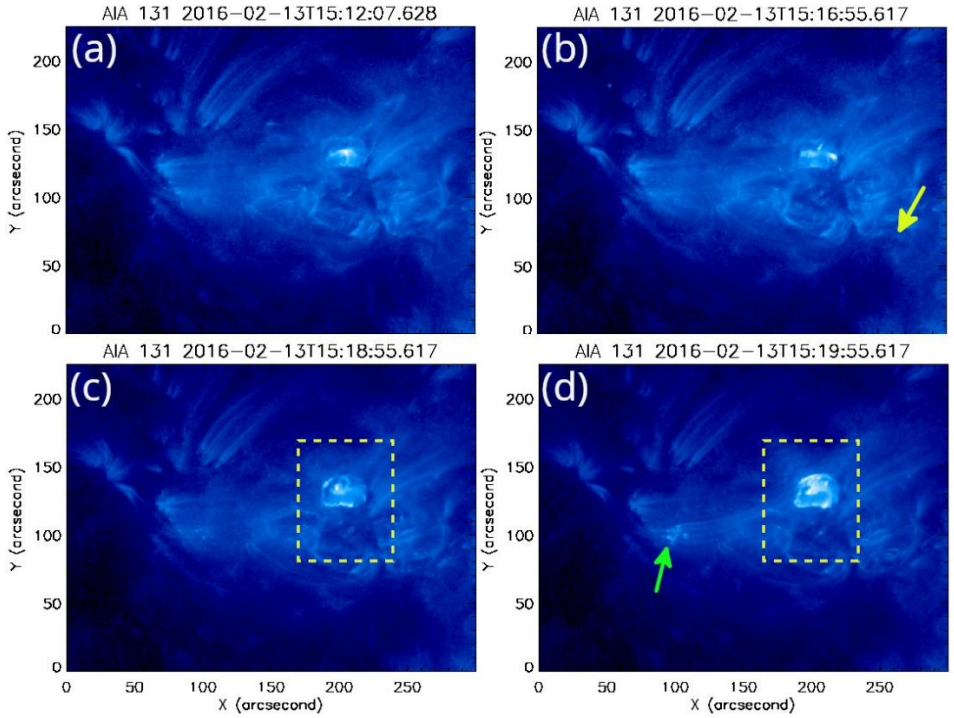

Figure 2: Temporal evolution of the solar active region observed by AIA onboard the SDO in the 131 Å channel on 13 February 2016. Panels (a)–(d) show the progression of the eruptive activity from 15:12:07 UT to 15:19:55 UT. The images reveal the development of bright hot coronal loops and flare structures associated with magnetic reconnection in the active region. The yellow arrow in panel (b) indicates the outward-moving plasma or expanding coronal structure, while the green arrow in panel (d) marks a secondary brightening or propagating feature. The dashed yellow boxes in panels (c) and (d) highlight the main flare core region where intense heating and magnetic restructuring are observed in the hot AIA 131 Å channel.

Figure 3 illustrates a series of observations from the chromosphere and transition region regarding the eruptive solar event that occurred on 13 February 2016. These observations were captured by the AIA/SDO, specifically in the 304 Å wavelength channel. The AIA 304 Å channel is primarily designed to detect emissions from He II plasma at temperatures ranging from approximately 50,000 to 80,000 K, making it particularly effective for examining filament activity, flare ribbons, chromospheric brightenings, and plasma movements within the lower solar atmosphere. This sequence demonstrates the temporal progression of the active region throughout the flare and eruption process, spanning from 15:12 UT to 15:19 UT. Panel (a), taken at 15:12:06 UT, depicts the active region prior to the significant eruption phase. The image reveals a well-defined system of bright chromospheric and transition-region loops that are distributed across the central area of the field of view. A compact bright core is discernible near X≈190″ and Y≈135″, signifying enhanced heating and localized energy release within the active region. The surrounding emissions exhibit twisted and sheared loop-like formations, indicating the existence of a complex magnetic configuration capable of storing considerable magnetic energy.

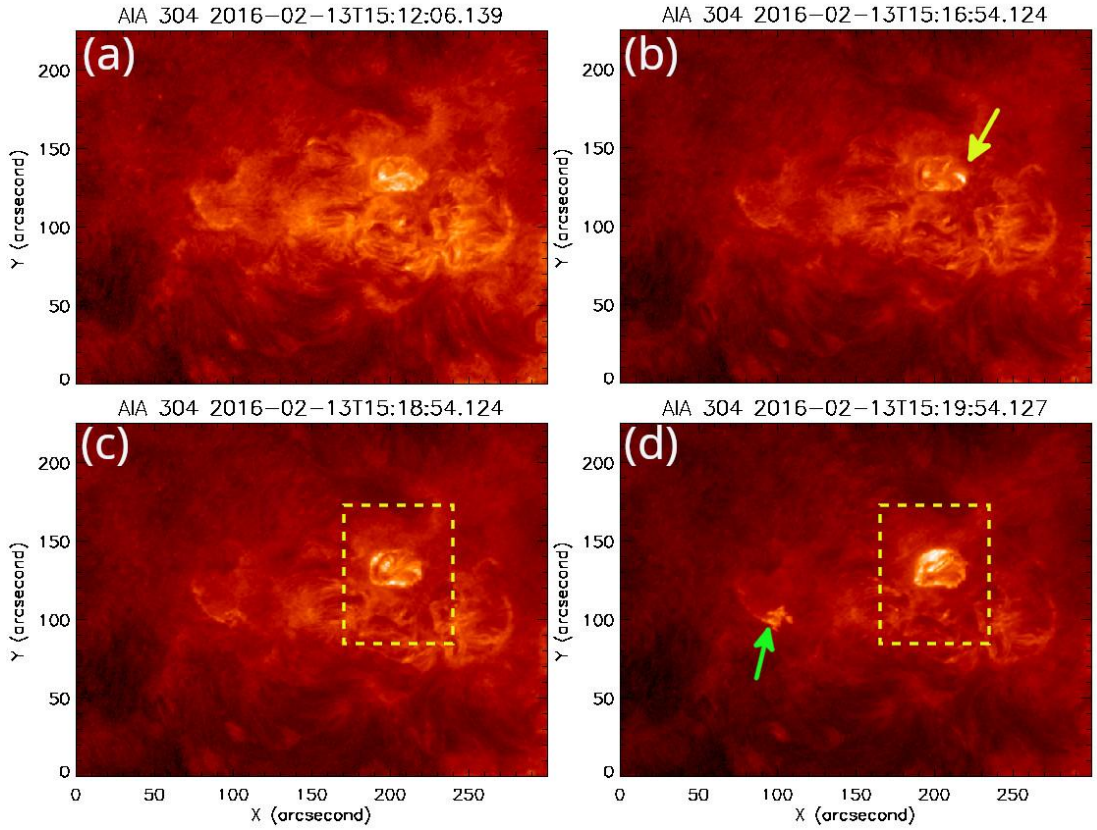

Figure 3: Panels (a)–(d) show the evolution of chromospheric and transition-region emission during the flare from 15:12:06 UT to 15:19:54 UT in the AIA 304 Å observations. The images reveal enhanced brightenings, evolving loop structures, and plasma dynamics associated with magnetic reconnection and flare energy release. The yellow arrow in panel (b) indicates a localized brightening associated with the activation of magnetic structures, while the green arrow in panel (d) marks a secondary bright feature or plasma ejection. The dashed yellow boxes in panels (c) and (d) highlight the principal flare core region exhibiting intense emission and magnetic restructuring in the AIA 304 Å observations.

In panel (b), captured at 15:16:54 UT, the active region displays evident dynamic evolution. The yellow arrow directs attention to a brightening feature situated in the upper-central area of the active region. This brightening is likely indicative of increased chromospheric heating or the activation of a magnetic loop system linked to the commencement of magnetic reconnection. The surrounding loop structures appear more disturbed in comparison to panel (a), suggesting rapid magnetic restructuring and plasma movement during the initial phase of the flare.

Panel (c), captured at 15:18:54 UT, demonstrates a notable increase in the intensity of the flare core region. The dashed yellow box delineates the main eruptive area where the most intense emission is focused. Within this boxed area, compact bright structures and loop-like features become more pronounced, signifying

significant heating in the chromosphere and transition region due to the deposition of flare energy. The heightened emission observed in the AIA 304 Å channel aligns with substantial plasma heating and a rise in particle precipitation into the lower solar atmosphere during the process of magnetic reconnection. Panel (d), documented at 15:19:54 UT, illustrates a further developed phase of the eruption. The green arrow points to a newly brightened compact feature located near X≈90″ and Y≈90″, which may be indicative of secondary energy release, plasma ejection, or the creation of newly reconnected magnetic loops. The flare core, contained within the dashed box, continues to brighten and evolve, implying persistent magnetic reconnection and ongoing energy release. The overall structure of the active region suggests a large-scale reconfiguration of the magnetic field throughout the eruptive event.

Figure 4 presents a series of four SDO/AIA 1600 Å images that illustrate the temporal progression of a localized solar atmospheric event occurring on 13 February 2016. The 1600 Å wavelength primarily captures emissions from the upper photosphere and transition region, rendering it particularly effective for identifying chromospheric brightenings, magnetic reconnection signatures, and small-scale eruptive phenomena. The four panels depict the spatial and temporal development of the event over a span of approximately eight minutes. In panel (a), observed at 15:11:51 UT, the region is relatively quiescent prior to the onset of transient activity. A compact magnetic structure is discernible near the center-right section of the image, characterized by a mix of bright and dark patches. These variations in intensity suggest underlying magnetic complexity, although no significant enhancement or eruption is yet apparent. This frame serves as the pre-event condition and acts as a baseline for comparison with subsequent stages. Panel (b), recorded at 15:16:39 UT, signifies the initiation phase of the event. The yellow arrow indicates a newly formed compact brightening situated above the central magnetic structure. The abrupt increase in ultraviolet emission implies localized plasma heating, which is typically associated with magnetic reconnection occurring in the lower solar atmosphere. The brightening appears restricted to a small area, suggesting the early release of magnetic energy prior to the event's further expansion. In panel (c), captured at 15:18:39 UT, the activity has progressed to a more developed stage. The brightened structure enlarges, becomes more intense, and exhibits greater morphological complexity. The dashed yellow box encompasses the core activity region, where the emission displays a loop-like or twisted configuration. Such structures frequently indicate the activation or destabilization of magnetic loops and the rapid reorganization of magnetic field lines. The increase in brightness signifies substantial energy deposition and enhanced emissions.

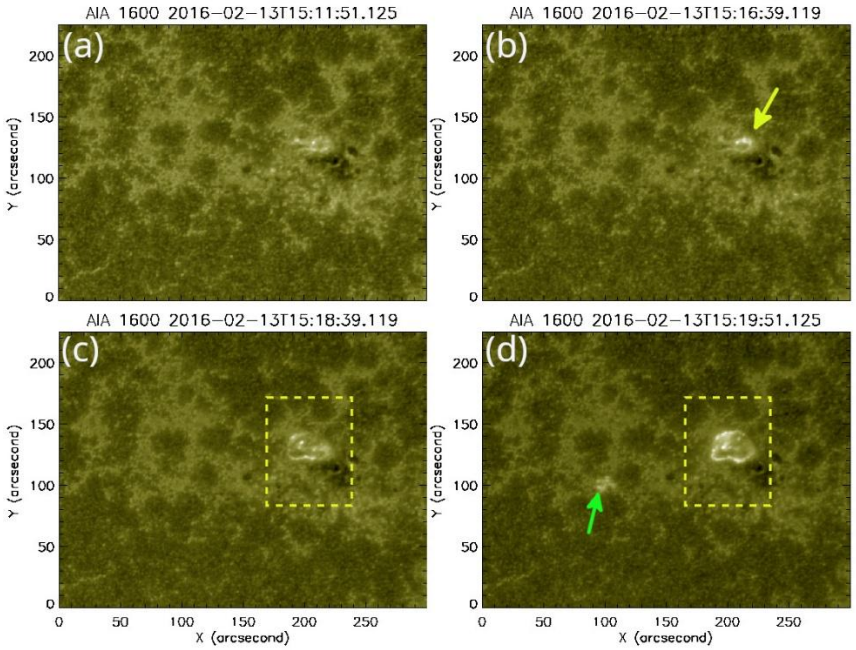

Figure 4: Sequence of solar EUV images at 1600 Å showing the temporal evolution of a localized brightening event on 13 February 2016. Panel (a) presents the pre-event stage with a relatively stable magnetic environment. In panel (b), the yellow arrow indicates the initial compact brightening, suggesting the onset of magnetic activity. Panel (c) shows the rapid expansion and intensification of the bright structure enclosed within the dashed yellow box, which is likely associated with magnetic reconnection and energy release in the lower solar atmosphere. In panel (d), the brightened region remains visible while the green arrow points to a secondary disturbance or propagating feature away from the main activity site. The sequence highlights the dynamic evolution of small-scale solar atmospheric activity over a timespan of several minutes.

Panel (d), observed at 15:19:51 UT, illustrates the later evolutionary phase of the event. The bright loop-shaped structure within the dashed box remains prominent, although its shape and intensity seem to evolve further as the system relaxes after the main energy release. The green arrow marks a secondary bright feature appearing away from the primary activity site. This feature may be related to the original reconnection event. Its appearance suggests that the energy release is not confined locally but may affect nearby regions through magnetic coupling.

3.2 Extrapolation from the Surface Magnetic Field

Figure 5 depicts a line-of-sight photospheric magnetogram of the solar active region captured at 15:12 UT before the flare eruption on 13 February 2016. This magnetogram was acquired from the HMI aboard the SDO and served as the lower boundary condition for conducting potential magnetic field extrapolation to explore the coronal magnetic configuration linked to the flare.

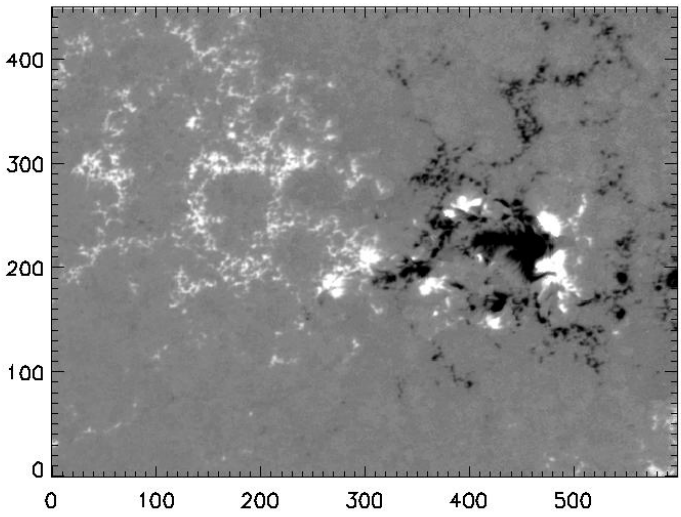

Figure 5: Pre-flare photospheric line-of-sight magnetogram of the active region observed at 15:12 UT on 13 February 2016 by the Helioseismic and Magnetic Imager (HMI) onboard the Solar Dynamics Observatory. The white and black regions represent positive and negative magnetic polarities, respectively. The magnetogram reveals a complex mixed-polarity magnetic configuration with strong magnetic gradients and polarity inversion regions associated with the flare source region. This magnetogram was used as the lower boundary condition for potential field extrapolation to investigate the coronal magnetic topology.

In the magnetogram, the bright and dark areas signify opposing magnetic polarities on the solar photosphere. The white areas represent positive magnetic flux, where the magnetic field is oriented outward from the solar surface, while the black areas denote negative magnetic flux, where the field is directed inward toward the Sun. The image displays a highly intricate and compact magnetic configuration primarily concentrated in the central-right section of the field of view. Clearly visible strong mixed-polarity regions indicate the presence of significant magnetic field gradients and polarity inversion lines (PILs), which are typically associated with active regions that produce flares. The central dark structure resembling a sunspot, encircled by bright magnetic concentrations, suggests the presence of a magnetically stressed active region characterized by considerable magnetic shear. The close proximity of opposite polarities indicates robust magnetic interaction and the potential for magnetic reconnection in the overlying corona.

Such configurations are advantageous for storing magnetic free energy, which can subsequently be released explosively during solar flares and eruptive events. The extended, weaker magnetic patches located toward the left side of the image signify dispersed magnetic flux linking the active region to adjacent coronal structures. These extensive magnetic connections are crucial for comprehending the global coronal topology and the development of the magnetic field associated with the flare.

This magnetogram is utilized for doing the potential field extrapolation to reconstruct the three-dimensional coronal magnetic field above the active region during the pre-flare stage. In the potential field approximation, the coronal magnetic field is assumed to be potential, i.e. current free, which satisfies:

$$\nabla \times \mathbf{B} = 0$$

and, therefore, the magnetic field to be expressed as the gradient of a scalar potential:

$$\mathbf{B} = -\nabla\phi$$

The extrapolation helps identify the large-scale magnetic connectivity, coronal loop systems, and possible regions of magnetic stress associated with the flare initiation.

Figure 6 depicts the three-dimensional extrapolation of the potential magnetic field for the flare-producing active region that was observed on 13 February 2016. This extrapolation utilized the pre-flare photospheric magnetogram acquired from the HMI at 15:12 UT. The extrapolated magnetic field lines are represented as red curves and are superimposed on both the photospheric magnetogram and the coronal EUV observations from AIA 131 Å channel. This figure demonstrates the extensive magnetic connectivity and the configuration of coronal loops associated with the eruptive flare region. Panel (a) presents a top-view projection of the extrapolated potential magnetic field lines overlaid on the HMI line-of-sight magnetogram. The regions depicted in white and black signify positive and negative magnetic polarities, respectively. The extrapolated field lines interconnect areas of opposing polarity, forming an arched loop system above the central active region. These field lines originate from the positive polarity area and conclude in the adjacent negative polarity concentrations, indicating robust magnetic connectivity across the polarity inversion line. The compact and curved shape of the loops implies the existence of a highly concentrated magnetic structure that is capable of storing magnetic energy prior to the flare eruption.

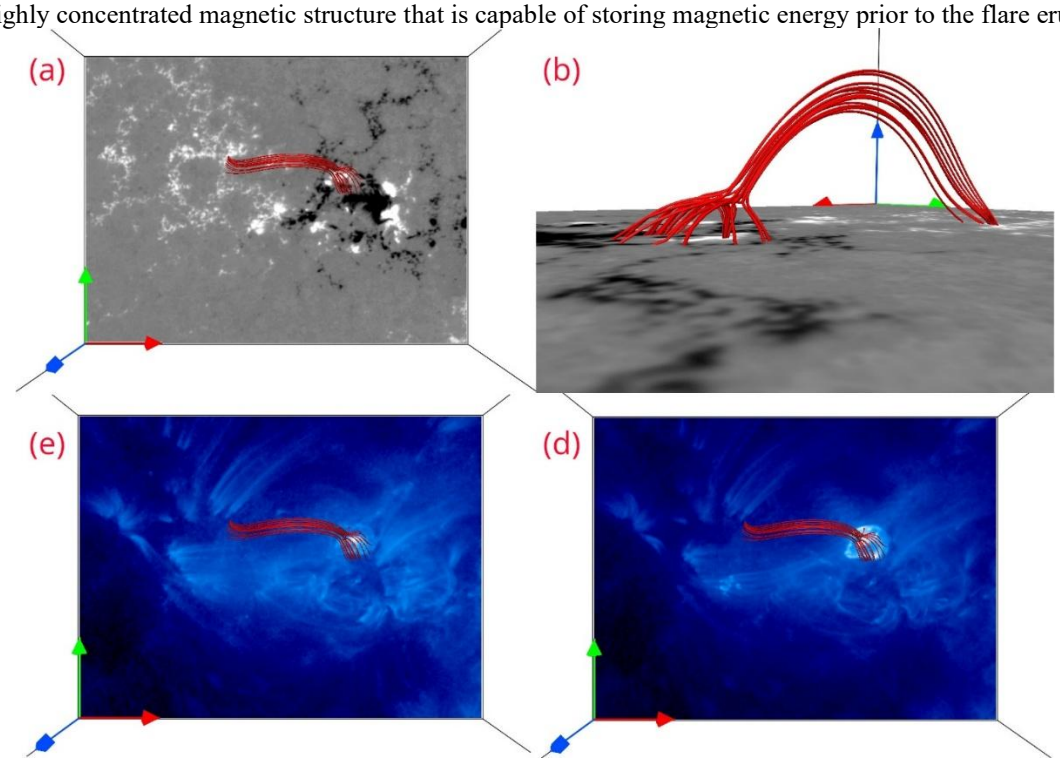

Figure 6: Potential magnetic field extrapolation of the flare-producing active region on 13 February 2016 using the pre-flare HMI line-of-sight magnetogram observed. The red curves represent the extrapolated magnetic field lines. Panel (a) shows the top-view projection of the extrapolated field lines overlaid on the HMI magnetogram, where white and black regions correspond to positive and negative magnetic polarities, respectively. Panel (b) presents the three-dimensional side-view of the extrapolated coronal magnetic loops. Panels (c) and (d) display the extrapolated field lines superimposed on the AIA 131 Å observations, showing good correspondence between the modeled magnetic structures and the observed hot coronal loops associated with the flare region.

Panel (b) illustrates a side-view perspective of the same extrapolated field lines, offering insight into the three-dimensional geometry of the coronal magnetic structure. The field lines ascend smoothly above the photospheric surface, forming a low-lying arcade-like configuration. The side-view indicates that the loop system exhibits significant curvature and height, suggesting extended magnetic connectivity within the corona. The lack of highly twisted or strongly sheared structures aligns with the principles of potential field extrapolation, where the magnetic field is regarded as current-free and relaxed towards a minimum-energy state. Panels (c) and (d) display the extrapolated magnetic field lines superimposed on the AIA 131 Å EUV images. The AIA 131 Å channel captures hot coronal plasma linked to flare loops and reconnection regions. The close spatial correlation between the extrapolated field lines and the observed coronal loops demonstrates that the potential extrapolation effectively replicates the large-scale magnetic connectivity of the active region. The extrapolated loops correspond well with the observed bright coronal structures extending from the flare core region towards the western side of the active region. In panel (d), the flare core is notably brighter due to increased heating and magnetic energy release during the eruptive phase. The extrapolated field lines remain anchored near the flare core and extend outward along the observed coronal structures, indicating that these magnetic loops likely contributed to the flare evolution and magnetic reconnection process. The consistency between the extrapolated field geometry and the observed EUV loops implies that the large-scale coronal magnetic field played a crucial role in directing plasma motion and regulating the flare dynamics.

IV. Summary and Conclusions

In this study, we conducted a comprehensive multiwavelength analysis of the confined solar flare that took place on 13 February 2016 in NOAA Active Region 2497, utilizing data from the Atmospheric Imaging Assembly (AIA) and the Helioseismic and Magnetic Imager (HMI) aboard the Solar Dynamics Observatory. The event was examined through AIA observations at 131 Å, 94 Å, and 304 Å, alongside photospheric magnetic field data from HMI, to gain insights into the temporal evolution, magnetic topology, and confinement mechanisms of the flare. Additionally, we performed potential magnetic field extrapolation using the pre-flare HMI magnetogram to reconstruct the large-scale coronal magnetic configuration linked to the region responsible for the flare.

The AIA observations indicated significant EUV brightenings, the formation of hot coronal loops, chromospheric activity, and dynamic reconfiguration of magnetic loops throughout the flare's evolution. The AIA channels at 131 Å and 94 Å displayed strong emissions from high-temperature plasma concentrated around the flare core, suggesting considerable heating due to magnetic reconnection in the corona. Furthermore, the 304 Å observations highlighted increased chromospheric and transition-region brightenings associated with flare ribbons and localized plasma movements in the lower solar atmosphere. The temporal evolution observed across various wavelengths illustrated a close interaction between the chromosphere and the overlying corona during the flare event. The GOES soft X-ray profile validated the occurrence of an M-class flare, exhibiting a gradual rise, peak, and decay phase corresponding to the energy release process. Despite the flare's significant coronal heating and magnetic restructuring, no successful large-scale eruption or coronal mass ejection (CME) was detected, confirming the event's confined nature. The lack of a CME, despite the strong flare emissions, suggests that the surrounding magnetic environment played a crucial role in inhibiting the eruption.

The HMI magnetogram displayed a complex mixed-polarity magnetic configuration characterized by strong magnetic gradients and regions of polarity inversion within the flare source area. This magnetic complexity is conducive to the accumulation of magnetic free energy and the onset of magnetic reconnection. The potential magnetic field extrapolation reconstructed a system of large-scale coronal loops that connect areas of opposite magnetic polarity. The extrapolated field lines were in good agreement with the observed coronal loops in the AIA EUV images, indicating that the extrapolation effectively reproduced the overall magnetic connectivity of the active region. The extrapolated magnetic structure suggested the existence of a stable overlying magnetic arcade situated above the flare core region. This overlying loop system likely functioned as a restraining magnetic cage, inhibiting the upward expansion of erupting plasma and preventing the successful development of a CME. Consequently, the observed confinement of the flare appears to be closely linked to the strength and geometry of the surrounding coronal magnetic field. These findings support earlier studies that propose confined flares occur when robust overlying magnetic fields suppress the eruption, despite significant magnetic energy release in the low corona.

In summary, this study illustrates that multiwavelength observations, when combined with magnetic field extrapolation, offer valuable insights into the physical processes that govern confined solar flares. The analysis underscores the essential role of coronal magnetic topology and overlying magnetic loop systems in determining

whether a flare will erupt or remain confined. Furthermore, the results highlight the significance of magnetic field studies in understanding flare dynamics, energy release, and the stability of solar active regions.

Acknowledgment
The authors wish express their gratitude to Dr. Sanjay Kumar for extending the computational resources available in his laboratory at the Department of Physics, Patna University, to carry out the extrapolation presented in this paper.

Funding

No funding

Data availability

National Aeronautics and Space Administration (NASA), Solar Dynamic Observatory (SDO).

Conflict of Interest
The authors declare that they have no known competing financial interests or personal relationships that could have appeared to influence the work reported in this work.

References

[1]. Priest, E. R., and Forbes, T. G. 2002, The magnetic nature of solar flares, Astronomy and Astrophysics Review, 10, 313–377.
[2]. Benz, A. O. 2017, Flare observations, Living Reviews in Solar Physics, 14, 2.
[3]. Fletcher, L., Dennis, B. R., Hudson, H. S., et al. 2011, An observational overview of solar flares, Space Science Reviews, 159, 19–106.
[4]. Schrijver, C. J. 2009, Driving major solar flares and eruptions: A review, Advances in Space Research, 43, 739–755.
[5]. Toriumi, S., and Wang, H. 2019, Flare-productive active regions, Living Reviews in Solar Physics, 16, 3.
[6]. Wang, Y., Zhang, J., Shen, C., et al. 2017, Statistical study of confined and eruptive flares, Journal of Geophysical Research: Space Physics, 122, 638–652.
[7]. Sun, X., Hoeksema, J. T., Liu, Y., et al. 2015, Why is the great solar active region 12192 flare-rich but CME-poor?, Astrophysical Journal Letters, 804, L28.
[8]. Thalmann, J. K., Su, Y., Temmer, M., and Veronig, A. M. 2015, The confined X-class flares of solar active region 2192, Astrophysical Journal Letters, 801, L23.
[9]. Jing, J., Tan, C., Yuan, Y., et al. 2018, Magnetic properties of confined solar flares, Astrophysical Journal, 864, 138.
[10]. Török, T., and Kliem, B. 2005, Confined and ejective eruptions of kink-unstable flux ropes, Astrophysical Journal Letters, 630, L97–L100.
[11]. Liu, Y. 2008, Magnetic conditions necessary for solar eruptions, Astrophysical Journal Letters, 679, L151–L154.
[12]. Guo, Y., Ding, M. D., Schmieder, B., et al. 2010, Driving mechanism and onset condition of confined eruptions, Astrophysical Journal, 725, L38–L42.
[13]. Wang, H., and Zhang, J. 2007, Observational evidence of back reaction on the solar surface associated with coronal magnetic restructuring, Astrophysical Journal, 665, 1428–1438.
[14]. Sweet, P. A. 1958, The neutral point theory of solar flares, IAU Symposium, 6, 123–134.
[15]. Petschek, H. E. 1964, Magnetic field annihilation, NASA Special Publication, 50, 425–439.
[16]. Shibata, K., and Magara, T. 2011, Solar flares: Magnetohydrodynamic processes, Living Reviews in Solar Physics, 8, 6.
[17]. Tsuneta, S. 1996, Structure and dynamics of magnetic reconnection in a solar flare, Astrophysical Journal, 456, 840–849.
[18]. Savage, S. L., McKenzie, D. E., and Reeves, K. K. 2012, Reconnection outflows and current sheet observations, Astrophysical Journal Letters, 747, L40.
[19]. Su, Y., Veronig, A. M., Holman, G. D., et al. 2013, Imaging coronal magnetic-field reconnection in a solar flare, Nature Physics, 9, 489–493.
[20]. Kushwaha, U., and Maurya, R. A. 2021, Multiwavelength analysis of confined solar flare dynamics, Solar Physics, 296, 71.
[21]. Lemen, J. R., et al. 2012, The Atmospheric Imaging Assembly (AIA) on the Solar Dynamics Observatory, Solar Physics, 275, 17–40.
[22]. O'Dwyer, B., Del Zanna, G., Mason, H. E., Weber, M. A., and Tripathi, D. 2010, SDO/AIA response to coronal hole, quiet Sun, active region, and flare plasma, Astronomy and Astrophysics, 521, A21.
[23]. Schou, J., et al. 2012, Design and ground calibration of the Helioseismic and Magnetic Imager (HMI) instrument on the Solar Dynamics Observatory, Solar Physics, 275, 229–259.
[24]. Wiegelmann, T., and Sakurai, T. 2012, Solar force-free magnetic fields, Living Reviews in Solar Physics, 9, 5.
[25]. Alissandrakis, C. E. 1981, On the computation of constant alpha force-free magnetic field, Astronomy and Astrophysics, 100, 197–200.
[26]. Gary, G. A. 1989, Linear force-free magnetic fields for solar extrapolation and interpretation, Astrophysical Journal Supplement Series, 69, 323–348.
[27]. Aschwanden, M. J. 2005, Physics of the Solar Corona: An Introduction, Springer Praxis Books.
[28]. Cheng, X., Ding, M. D., Zhang, J., et al. 2011, Observing flux rope formation during the impulsive phase of a solar eruption, Astrophysical Journal, 732, L25.
[29]. Ji, H., Wang, H., Schmahl, E. J., et al. 2003, Observations of the failed eruption associated with an X-class flare, Astrophysical Journal Letters, 595, L135–L138.
[30]. Netzel, A., Mrozek, T., and Kołomański, S. 2012, Characteristics of confined solar flares observed by RHESSI, Astronomy and Astrophysics, 548, A89.
[31]. Kliem, B., and Török, T. 2006, Torus instability, Physical Review Letters, 96, 255002.